Journal of the Korean Physical Society, Vol. 72, No. 2, January 2018, pp. 254∼259

Comparative Study of Epitaxial Lateral Overgrowth on Semipolar (11-22) GaN by Using Stripe and Hexagon SiO_2 Mask Patterns

Hyunseok Na
Department of Materials Science and Engineering, Daejin University, Pocheon 11159, Korea

Ki-Ryong Song, Jae-Hwan Lee, Sang-Hyun Han and Sung-Nam Lee*
Department of Nano-Optical Engineering, Korea Polytechnic University, Siheung 15073, Korea

(Received 6 September 2017)

We investigated defect reduction of epitaxial lateral overgrown (ELO) semipolar (11-22) GaN grown on m-plane sapphire substrate by using stripe and hexagon SiO_2 patterns. We obtained the fully-coalescent semipolar ELO-GaN templates successfully regardless of pattern shape and size. However, ELO-GaN film grown on hexagonal patterns were more easily coalesced than ELO-GaN grown on stripe patterns during ELO process due to the lateral growths from six directions. X-ray rocking curves from ELO-GaN films indicate that ELO-GaN had much better crystal quality than GaN template. However, the effect of the lateral overgrowth on hexagon patterns on crystal quality was limited because the large frictions from the six-directional growth on hexagon pattern resulted in crystallographic tilts. The photoluminescence emissions of donor-bound exciton (D^0X) recombination were observed from both samples, but the D^0X emission of stripe ELO-GaN film was considerably stronger than that of hexagon ELO-GaN. In addition, the defect-related emissions of stripe ELO-GaN were also weaker, indicating that stripe ELO-GaN has efficiently eliminated the non-radiative centers and suppressed the defects.

PACS numbers: 68.55.J−, 78.55.Cr, 81.15.Gh
Keywords: GaN, Semipolar, ELO, XRD
DOI: 10.3938/jkps.72.254

I. INTRODUCTION

GaN-based semiconductors exhibit the wide range of bandgap energy, which offer the possibility to cover all the visible spectral range for optical applications [1]. Recently, the growth of GaN films oriented along nonpolar and semipolar directions have been receiving considerable attention to alleviate the spontaneous and strain-induced piezoelectric polarization effects that are inherent to the *c*-axis-oriented GaN [2]. Semipolar (11-22) plane was tilted by 58.4° with respect to (0001) plane, and internal polarization is reduced to 1/3 compared to (0001) GaN [3]. However, it was well-known that the semipolar (11-22) GaN grown on the m-plane (10-10) sapphire had poor crystal quality with partial dislocations (PDs) of $\sim 10^{10}$ cm^{-2}, basal stacking faults (BSFs) of $\sim 10^5$ cm^{-1}, and prismatic stacking faults (PSFs) [4], which could act as non-radiative recombination centers. Currently, the best performance of semipolar GaN-based LED/LDs has been achieved by using high quality semipolar GaN substrate with much lower TDs and BSFs [5,6], but this substrate has the disadvantages of very high price and small size.

The epitaxial-lateral overgrowth (ELO) technique has been adapted for better material quality in GaN heteroepitaxy on sapphire decreasing the density of point defects and dislocations [7, 8]. Recently, remarkable progress in nonpolar and semipolar GaN growth has been also reported by adapting conventional ELO technique [9,10]. However, most reports have focused on the growth behavior on stripe SiO_2 pattern with different width and the characterization of crystal quality. In addition, it reported that the ELO with the hemispherical SiO_2 pattern was studied to reduce the crystal defect and to increase the extraction efficiency from reflecting the interface between GaN and sapphire substrate [11]. In this paper, we investigated comparatively the effect of growth behavior on different SiO_2 pattern shapes by using the stripe and the hexagon patterns which would affect the lateral coalescence and the crystal quality of semipolar (11-22) GaN.

*E-mail: snlee@kpu.ac.kr

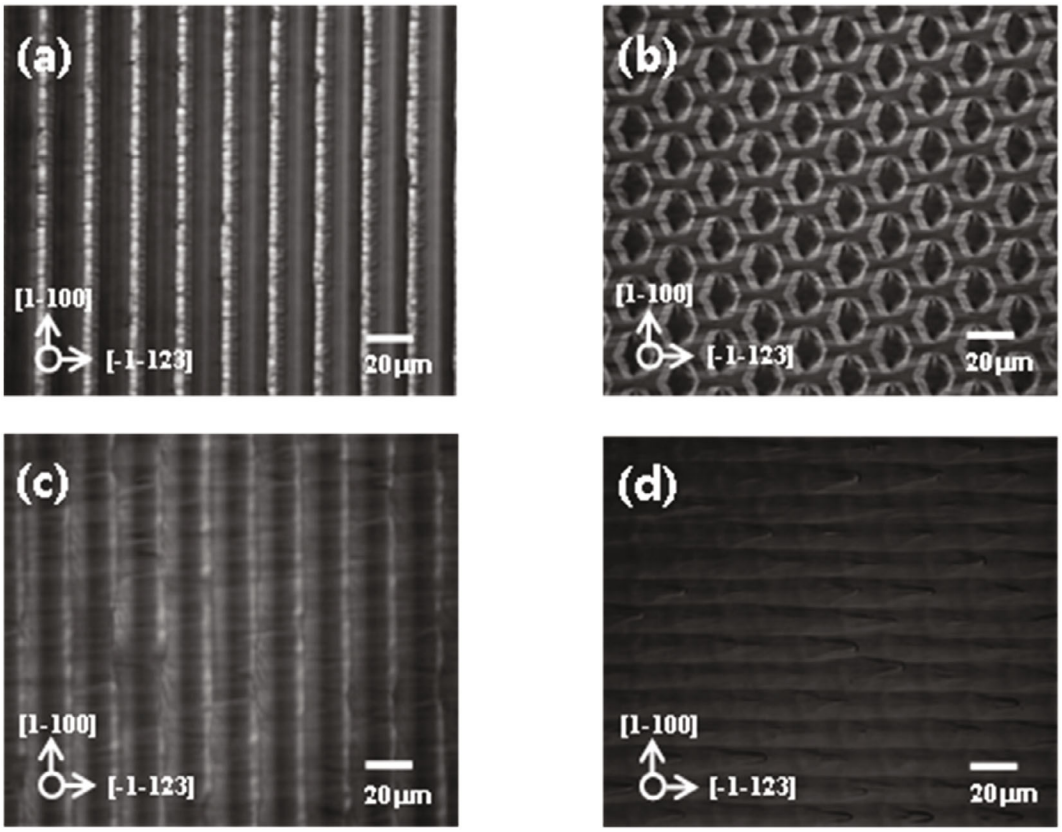

Fig. 1. Optical microscope images for the non-merged ((a) and (b), [13]) and fully-coalesced ((c) and (d)) semipolar (11-22) ELO-GaN films with the stripe and the hexagon patterns, respectively.

II. EXPERIMENTS

We prepared 2.0 μm-thick semipolar (11-22) GaN epilayer grown on m-plane sapphire substrate by using the high temperature one-step growth method instead of the typical two-step growth procedure of metalorganic chemical vapor deposition (MOCVD) [12]. The semipolar (11-22) undoped GaN template was grown at 1030 °C and 80 Torr with the V/III ratio of 1165. 100 nm-thick SiO_2 films were deposited on the semipolar (11-22) GaN templates by using plasma-enhanced chemical vapor deposition (PECVD) system, and then the stripe and the hexagon patterns were formed by the standard photolithography and the wet etching process. The SiO_2 stripe patterns consisted of 12.0 μm mask and 4.0 μm opening, and SiO_2 stripes were oriented along the [1-100] direction (perpendicular to the *c*-axis). The SiO_2 hexagon patterns consisted of 15.0 μm-wide hexagon mask and 4.0 μm opening [13].

To obtain the semipolar ELO-GaN film, both samples with two patterns were loaded at the same time and grown under identical condition in MOCVD reactor. Growth temperature was kept at 1030 °C during the entire process. Trymethylgallium (TMGa) and ammonia (NH_3) were used as the Ga and N sources, respectively. The ELO-process consisted of three steps growth technique [14]. The first step was the growth of GaN seed at the opening region under the same growth condition of semipolar GaN template. The second step was the lateral growth of GaN for coalescence under the reactor pressure of 300 Torr, and the V/III ratio was drastically reduced down from 1165 to 580. The last step was the planarization growth, and V/III ratio was changed to 1165 again in order to obtain smooth surface after coalescence [15].

The surface morphology of semipolar ELO-GaN film was observed by the optical microscope (OM), the atomic force microscope (AFM), and the scanning electron microscope (SEM). The crystal qualities of semipolar (11-22) ELO-GaN epilayers were characterized by high-resolution X-ray diffraction (HR-XRD) with the different incident beam directions of [1-100] and [-1-123]. The optical properties of semipolar ELO-GaN were investigated by low temperature photoluminescence (LT-PL) analysis at 13 K using 325 nm line of He-Cd laser.

III. RESULTS AND DISCUSSION

Figures 1(a) - (d) show OM images for the non-merged and fully-coalesced semipolar ELO-GaN films with the stripe and the hexagon patterns on m-plane (10-10)

sapphire substrates. As shown in Figs. 1(a) and (b), we found that, for non-merged ELO-GaN films that stopped the growth in the middle of the second step, the hexagon-patterned ELO-GaN film was partially coalesced, while the stripe-patterned ELO-GaN was still not coalescenced. It indicates that ELO-GaN on hexagon pattern was coalesced more easily than ELO-GaN on stripe pattern. It is well-known that the enhanced growth rate along the +c direction leads to overgrowth on top of adjacent [1-100]-aligned SiO_2 stripe [16]. However, the lateral growth of semipolar GaN proceeded in six directions of hexagon mask. In spite of the difficulties of lateral growth on the hexagon ELO pattern, we successfully achieved that semipolar ELO-GaN films were fully coalesced on stripe and hexagon patterns after the last planarization growth step as shown in Figs. 1(c) and (d).

Figure 2 shows the result of AFM images of fully-coalesced ELO-GaN on the stripe and the hexagon patterns. The microscopic surface demonstrates clearly that ELO-GaN on stripe pattern had typical coalescence, seed, and wing regions [14], while ELO-GaN on hexagon pattern had the small arrowhead-like surface structure only without any specific region. Root-mean-square (RMS) roughness of stripe and hexagon ELO-GaN were 14.0 nm and 9.88 nm, respectively. RMS roughness of coalescence/seed region (region A) and wing region (region B) of Fig. 2(a) were 7.4 nm and 4.5 nm, respectively, and we confirmed that the region A of coalescence/seed was rougher than region B of wing. However, in the hexagon ELO-GaN film, coalescence/seed and wing regions were clearly observed. As a result, we surmise that ELO-GaN on stripe pattern had rougher surface than ELO-GaN on hexagon pattern due to the existence of the coalescence boundaries of ELO-GaN film. In addition, we believed that the hexagon-patterned ELO-GaN was easily coalesced due to the lateral growth from six directions.

Figures 3(a) - (d) show the cross-sectional SEM images of the non-merged and fully-coalesced semipolar ELO-GaN films with the stripe and the hexagon patterns grown on m-plane (10-10) sapphire substrates. It reported that the growth process of stripe ELO-GaN coexists with difference facets (*a*-plane, +*c*-plane and semipolar (11-22) plane) as confirmed in Fig. 3(a) [14]. In that case, the growth rate toward the +*c*-direction was significantly enhanced, allowing the crystal to grow above its adjacent neighbor, which was consistent with the result of Fig. 2(a). The surface structure of coalescence/seed GaN region in Fig. 2(a) appears clearly along the main growth direction (+*c*-direction). It was also well-known that voids of equilateral triangle shape were formed in fully-merged ELO-GaN on stripe pattern as shown Fig. 3(b) [17]. Figures 3(c) and (d) showed that the growth mode of ELO-GaN on hexagon pattern was significantly different from ELO-GaN on stripe pattern. The main growing direction of ELO-GaN on hexagon pattern was also +*c*-direction, but we found many facets in various directions of hexagon shape. This implies that

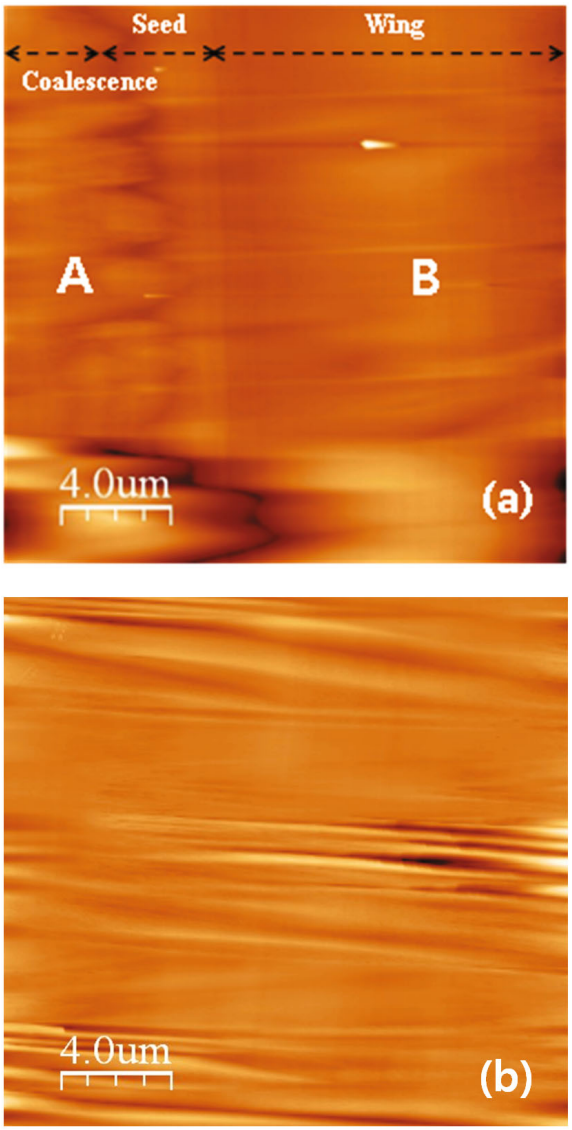

Fig. 2. (Color online) AFM images (20 × 20 μm) for fully coalescence of (a) stripe and (b) hexagon [13] ELO-GaN films.

the growth process occurred in six directions of hexagon shape including +*c*-axis. In addition, we found that the void height of fully-coalesced ELO-GaN on stripe and hexagon patterns reached 5.5 and 4.5 μm, respectively, indicating that hexagon ELO-GaN could be coalesced easily.

Figures 4(a) and (b) show X-ray rocking curves (XRCs) obtained from fully-merged (11-22) ELO-GaNs on the stripe and the hexagon pattern with different two X-ray beam incident directions of [-1-123] and [1-100], respectively. The full width at half maximum (FWHM) values of ELO-GaN films on the stripe and the hexagon patterns were 537 and 892 arcsec for XRC in [-1-123] direction, respectively. Moreover, the XRC FWHMs of the stripe and hexagon ELO-GaN films were 367 and 1078 arcsec in the X-ray beam direction of [1-100], re-

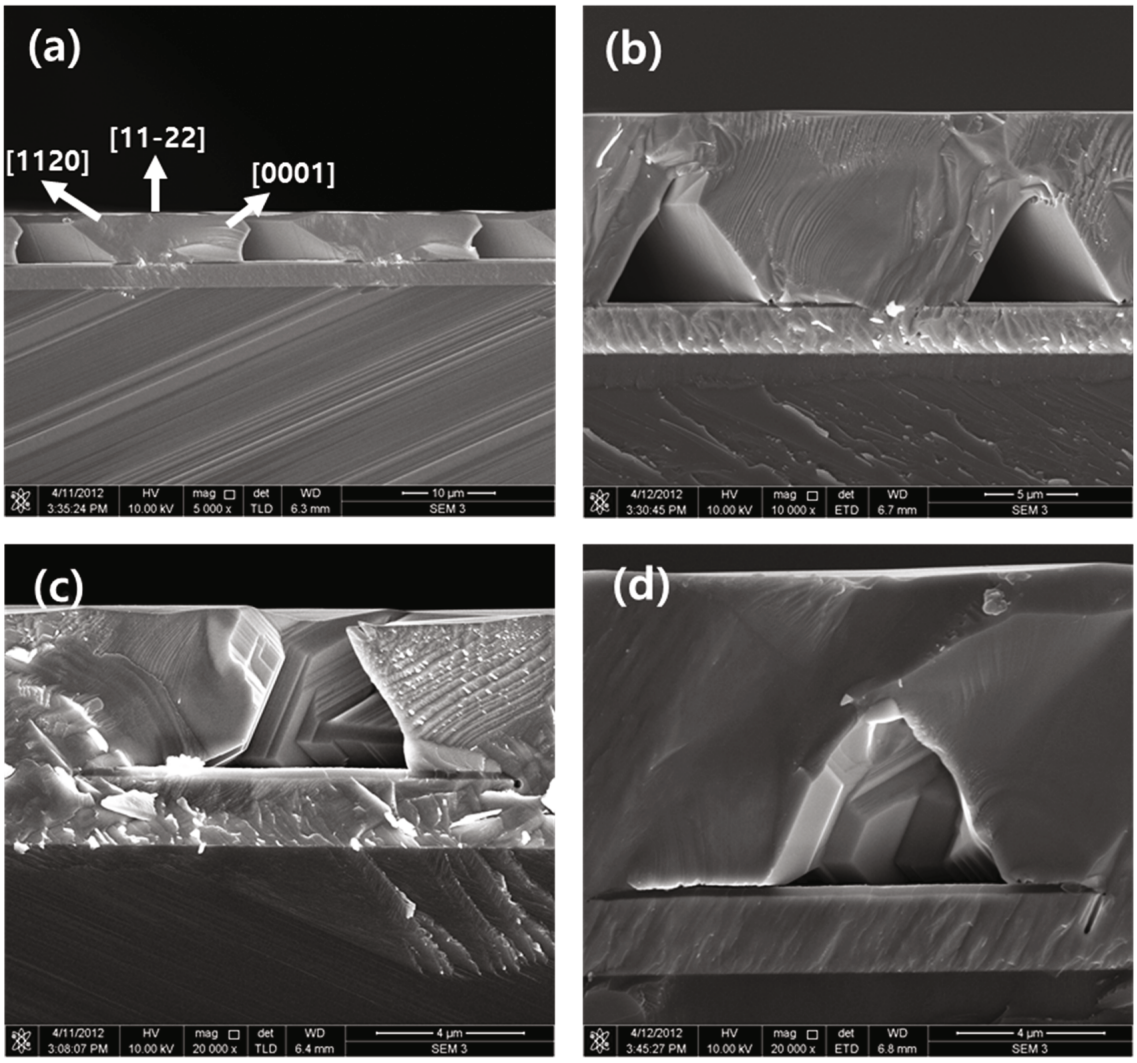

Fig. 3. Cross-sectional SEM images for the non-merged ((a) and (c)) and fully-coalesced ((b) and (d) [13]) semiplar (11-22) ELO-GaN films with stripe and hexagon patterns, respectively.

spectively. These results mean that the ELO-GaN films had much better crystal quality than semipolar (11-22) GaN template with FWHMs of $\sim$ 1200 arcsec in [-1-123] and $\sim$ 1500 arcsec in [1-100] in Fig. 6. Furthermore, regardless of x-ray incident beam directions, the crystal quality of ELO-GaN film was better on stripe-ELO pattern than hexagon-ELO pattern, even though the surface roughness of stripe-ELO GaN film was a little worse than that of hexagon-ELO GaN as shown in Fig. 2. However, the XRC FWHM of the stripe-ELO GaN in the [-1-123] direction was larger than that in the [1-100] direction, while the XRC FHWM of the hexagon-ELO GaN for [-1-123] direction was smaller than that in [1-100] direction. The stripe-ELO GaN grows laterally only in the [-1-123] direction, whereas the hexagon-ELO GaN grows laterally in three directions around [-1-123] perpendicular to [1-100]. Therefore, we guess that there is more crystallographic tilts toward [1-100] in the hexagon-ELO GaN films. In addition, one shoulder peak of the XRC in [-1-123] direction peak was observed from only hexagon-ELO GaN. It was presumed that the shoulder peak can be caused by distinctive morphology and crystallographic tilt at the coalesced region of hexagon-ELO GaN due to the lateral growths from six directions.

Figure 5 shows the FWHM values of XRCs obtained from semipolar (11-22) GaN template, stripe and hexagon ELO-GaN films as a function of the azimuth angles from 0°. The sample was rotated counterclockwise to change the azimuth angle with respect to the [1-100] direction. It is well known that the semipolar (11-22) GaN film showed W-shaped curve of XRC FHMWs due to the anisotropic crystallographic properties of semipolar (11-22) GaN film [18]. Regardless of stripe and hexagon ELO process, semipolar (11-22) GaN template and ELO-GaN film show the W-shape of the XRC FWHMs as a function of azimuth angle. In particular, the wing tilt was the major broadening mechanism for the stripe ELO-GaN film. It is interesting that the

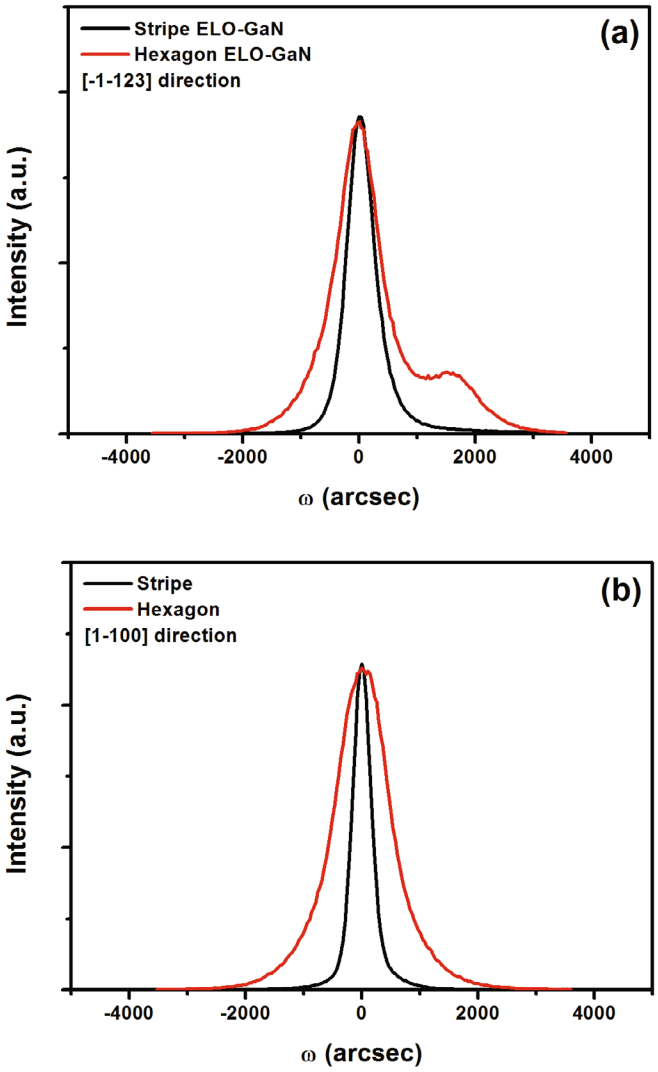

Fig. 4. (Color online) X-ray rocking curves of fully-merged semipolar (11-22) ELO-GaN films with the stripe and hexagon patterns along (a) [-1-123] direction and (b) [1-100] direction.

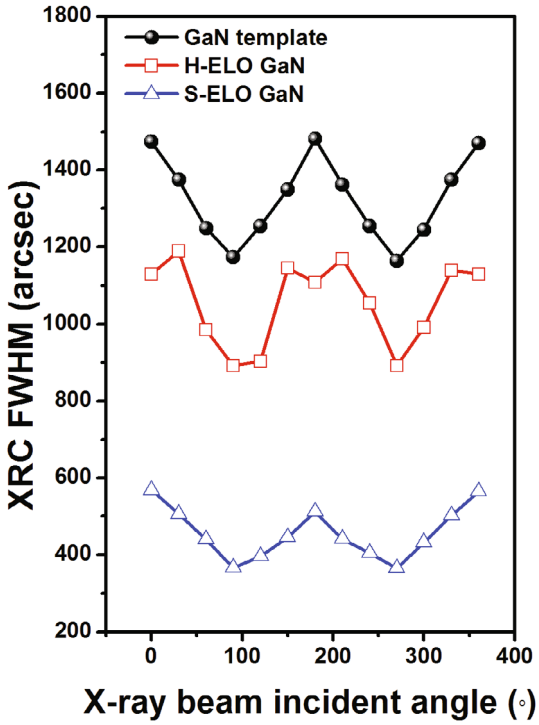

Fig. 5. (Color online) The FWHM values of XRCs obtained from (11-22) semipolar GaN template and ELO-GaN films on stripe and hexagon patterns as a function of the azimuth angles from [1-100].

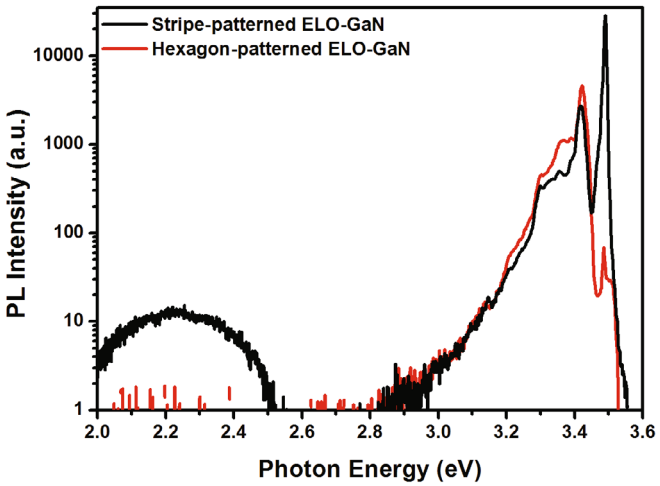

Fig. 6. (Color online) Low temperature (13 K) photoluminescence spectra from semipolar (11-22) ELO-GaN films on the stripe and the hexagon patterns.

hexagon-ELO GaN film has a W-shape curve shape similar to the stripe-ELO GaN film. It was presumed that this W-shape behavior was caused by the anisotropic crystallographic tilt of semipolar (11-22) GaN film and the coalesced GaN region on the stripe and hexagon patterns.

Figure 6 shows the luminescence property of semipolar (11-22) stripe and hexagon ELO-GaN epilayers characterized by LT-PL at 13 K using 325 nm He-Cd laser. The PL emission of stripe and hexagon ELO-GaN films showed the strong band-edge emissions by donor-bound exciton (D^0X) recombination at 3.489 eV [19], but the D^0X emission of stripe ELO-GaN film was considerably stronger than that of hexagon ELO-GaN. In addition, three additional emissions were observed at 3.42, 3.35 and 3.30 eV in both samples which were ascribed to the luminescence from BSFs, PSFs, and PDs, respectively [16,20]. These emissions of stripe ELO-GaN were weaker than that of hexagon ELO-GaN, indicating that the stripe ELO process has efficiently eliminated by suppressing the defects such as BSF, PSF, and PD as the non-radiative centers. However, only the stripe ELO-GaN showed the emission at 2.25 eV which was related to Ga vacancy [21]. We believed that many Ga vacancies were formed by lateral growth on stripe SiO_2 mask re-

gion causing crystallographic friction between GaN and SiO_2 mask, whereas it was not severe on hexagon SiO_2 pattern due to the relative discrete hexagon island pattern .

IV. CONCLUSION

We investigated the growth modes, crystal properties, and optical properties of semipolar (11-22) ELO-GaN films with different pattern shapes. The surface morphology of stripe ELO-GaN was rougher than that of hexagon-ELO GaN, and the hexagon-ELO GaN was easily coalesced due to the lateral growths from six directions on the hexagon SiO_2 patterns. We found that the main lateral growth direction of hexagon-ELO GaN was toward the $+c$-direction, but there were many facets in various directions of hexagon shape. Regardless of pattern shapes, ELO-GaN films had much better crystal quality than semipolar (11-22) GaN template. However, the crystal quality of ELO-GaN was better on stripe than hexagon pattern. Stripe- ELO GaN film showed the stronger band-edge emission and the weaker defect-related emissions than hexagon-ELO GaN film. These results mean that the growth of hexagon-ELO GaN film had great advantage on the coalescence and the surface flatness, but it had disadvantage on the crystal quality and the optical property as confirmed with XRD and PL.

ACKNOWLEDGMENTS

This work was supported by a Research Program (NRF-2017R1D1A1B03031311) through the National Research Foundation (NRF) of Korea funded by the Ministry of Education, Science and Technology, and by Human Resources Program in the Transportation Specialized Lighting Core Technology Development (No. N0001364) granted financial resource from the Ministry of Trade, Industry and Energy, Republic of Korea.

REFERENCES

[1] S. Nakamura, G. Fasol and S. J. Pearton, *The Blue Laser Diode* (Springer, New York, 2000).
[2] T. Deguchi, K. Sekiguchi, A. Nakamura, T. Sota, R. Matsuo, S. Chichibu and S. Nakamura, Jpn. J. Appl. Phys., Part 2 **38**, L914 (1999).
[3] A. E. Romanov, T. J. Baker, S. Nakamura and J. S. Speck, J. Appl. Phys. **100**, 023522 (2006).
[4] T. J. Baker, B. A. Haskell, F. Wu, J. S. Speck and S. Nakamura, Jpn. J. Appl. Phys. **45**, L154 (2006).
[5] H. Sato, A. Tyagi, H. Zhong, N. Fellows, R. Chung, M. Saito, K. Fujito, J. S. Speck, S. P. DenBaars and S. Nakamura, Phys. Status. Solidi (RRL) **1**, 162(2007).
[6] Y. Enya, Y. Yoshizumi, T. Kyono, K. Akita, M. Ueno, M. Adachi, T. Sumitomo, S. Tokuyama, T. lkegami, K. Katayama and T. Nakamura, Appl. Phys. Express **2**, 082101 (2009).
[7] S. N. Lee, H. S. Paek, H. Kim, Y. M. Park, T. Jang and Y. Park, Appl. Phys. Lett. **92**, 111106 (2008).
[8] X. Ni, U. Ozgur, A. A. Baski, H. Morkoc, L. Zhou, D. J. Smith and C. A. Tran, Appl. Phys. Lett. **90**, 182109 (2007).
[9] M. D. Craven, S. H. Lim, F. Wu, J. S. Speck and S. P. Den Baars, Appl. Phys. Lett. **81**, 1201 (2002).
[10] M. D. Craven, S. H. Lim, F. Wu, J. S. Speck and S. P. DenBaars, Phys. Status Solidi A **194**, 541 (2002).
[11] M. Yamada, T. Mitani, Y. Narukawa, S. Shioji, I. Niki, S. Sonobe, K. Deguchi, M. Sano and T. Mukai, Jpn. J. Appl. Phys. **41**, L1431 (2002).
[12] M. Araki, N. Mochimizo, K. Hoshino and K. Tadatomo, Jpn. J. Appl. Phys. **46**, 555 (2007).
[13] J. H. Lee, S. H. Han, K. R. Song, J. H. Ryou, H. Na and S. N. Lee, Microelectron. Eng. **168**, 32 (2017).
[14] S-N. Lee, J. Kim and H. Kim, J. Electrochemical Society **158**, H994 (2011).
[15] X. Ni, U. Ozgur, A. A. Baski, H. Morkoc, Lin Zhou, David J. Smith and C. A. Tran, Appl. Phys. Lett. **90**, 182109 (2007).
[16] B. Lacroix, M. P. Chauvat, P. Ruterana, G. Nataf and P. de Mierry, Appl. Phys. Lett. **98**, 121916 (2011).
[17] N. Kriouche, P. Venne'gues, M. Nemoz, G. Nataf and P. De Mierry, J. Cryst. Growth **312**, 2625 (2010).
[18] J. H. Kim, S. M. Hwang, J. S. Son, K. H. Baik, K. M. Song and J. H. Park, J. Cryst. Growth **355**, 101 (2012).
[19] T. Gühne, Z. Bougrioua, P. Vennéguès, M. Leroux and M. Albrecht, J. Appl. Phys. **101**, 113101 (2007).
[20] R. Liu, A. Bell, F. A. Ponce, C. Q. Chen, J. W. Yang and M. A. Kahn, Appl. Phys. Lett. **86**, 021908 (2005).
[21] H. Xu, X. Hu, X. Xu, Y. Shen, S. Qu, C. Wang and S. Li, Appl. Surf. Sci. **258**, 6451 (2012).